Armenian Journal of Physics, 2011, vol. 4, issue 2, pp. 109-133

CORRELATION BETWEEN CRYSTAL STRUCTURE AND RESISTIVITY OF HIGH-TEMPERATURE SUPERCONDUCTING CUPRATES

H. P. Roeser[1*], A. Bohr[1], D. T. Haslam[1], J. S. López[1], M. Stepper[1], F. M. Huber[2], A. S. Nikoghosyan[3]

[1]*Institute of Space Systems, University of Stuttgart, Pfaffenwaldring 29, 70569 Stuttgart, Germany*

[2]*German Aerospace Center, GSOC, Muenchnerstr. 20, 82234 Wessling, Germany*

[3]*Department of Microwave and Telecommunication, Yerevan State University,*

Alex Manoogian 1, Yerevan, 0025, Armenia

**E-mail address:* roeser@irs.uni-stuttgart.de

Received 24 July, 2011

Abstract–The experimental resistivity of high-temperature superconducting (HTSC) cuprates at about T_c has been determined by many authors. For large devices the in-CuO_2-plane resistivity has a range of $(\sim 0.5 < \rho(\exp) <\sim 1.5)\times 10^{-6}$ Ω m. Above T_c all HTSC materials behave like a classical device and the resistance depends on cross section and length of the device. Assuming a superconducting unit volume and a mode structure, which are given by the doping pattern throughout the whole crystal, the experimental resistivity values have been plotted versus $\sim L_R/N_{\mathrm{mode}}$. A strong linear correlation in the form $\rho(\exp) = m_3\left(L_R/N_{\mathrm{mode}}\right)\left(n_4/n_3\right)$ can be seen with a slope of $m_3 = (13.39 \pm 0.79)\times 10^3$ Ω. L_R is an effective resistivity length, N_{mode} is the number of CuO_2 planes per unit cell, n_3 is the number of Cu^{3+}-ions per chemical formula and n_4 is the number of different shifted stacking sequences per unit cell. The investigation has only been performed for a maximum of $N_{\mathrm{mode}} = 4$ modes. The value for m_3 is very close to the fundamental resistance of a single-mode ballistic conductor $R_{sm} = h/2e^2 \approx 12,906$ Ω, which appears when size quantization plays a dominant role.

Keywords: superconducting unit volume, superconducting current channels, superconducting waveguide, resistivity of cuprates

1. Introduction

An important indication of superconductivity is given by the fact that at a particular physical temperature T_c the resistance of a superconducting material vanishes completely or gets extremely small. This phenomenon is known since its discovery by Heike Kamerlingh Onnes in 1911 and is one of the most interesting and sophisticated problems in condensed matter physics. Since about 1985, high temperature superconductors (HTSC) offer additional experimental data up to 135 K which are much more convenient to achieve compared to conventional superconductors with much lower T_c. Many experts are still searching for an explanation for the unusual temperature dependences of the electric resistivity ρ: why does the resistivity for some materials disappear at a certain fixed temperature or what is so special of ρ at T_c from the standpoint of its normal conducting state?

This paper is an attempt to find a relation between the experimental resistivity value at about T_c and the crystal structure of optimum doped HTSC materials.

2. Doping Structure in high-temperature superconductors

For HTSCs doping is necessary to make the parent material superconducting and each HTSC material has an optimum doping level for maximum T_c. Recently the authors have found a correlation between the maximum critical transition temperature T_c and the doping distance x assuming a uniform doping distribution [1] leading to a relation

$$(2x)^2 n_1^{-2/3} 2M_{\text{eff}} \pi k T_c \approx h^2. \quad (1)$$

This demonstrates the important role of the crystal structure and the super lattice of the uniform doping structure. In cuprates the superconducting carriers have an effective mass $M_{\text{eff}} = 2m_e$ and the CuO_2 planes act as the superconducting highway. As an example Fig. 1a shows the situation for Hg-1201 with $T_c \approx 95$ K and $n_1 = 1$ CuO_2 plane per unit cell. It is suggested that superconducting current channels are formed by straight lines of equidistant doped unit cells separated in the CuO_2 plane by a distance *x*. Therefore, Hg-1201 is considered here as a bundle of parallel superconducting current channels with cross section $A_{SC} = W_{SC} \times H$ throughout the whole crystal. The height is given by the separation of two CuO_2 planes ($H = c$). Figure 1a also suggests defining a superconducting unit volume $V_{SC} = A_{SC} \times L_{SC}$, which results in $V_{SC} = cx^2$ for Hg-1201 with $L_{SC} = W_{SC} = x$. If the whole HTSC crystal is made up of these unit blocks this results in a doping density of $N_D = 1/V_{SC}$ (m^{-3}) and charge density of $N_e = 2N_D$, respectively because $M_{\text{eff}} = 2m_e$.

3. Resistivity and single-mode conductors

The resistance *R* of a "classical" and macroscopic device with length *L* and cross section *A* is given by

$$R = \frac{1}{\sigma}\frac{L}{A} = \rho\frac{L}{A} \quad (2)$$

with conductivity σ or resistivity ρ as an intrinsic property of the material. The conductivity is also used as the proportionality factor between current density *J* and the electric field *E* causing the current flow ($J = \sigma E$) with

$$\rho = \frac{1}{\sigma} = \frac{m_e}{N_e e^2 \tau} = \frac{1}{N_e e}\frac{1}{\mu}, \quad (3)$$

where N_e is the carrier density, τ the mean time between collisions and $\mu = \tau e/m_e$ the mobility of the carriers.

For an undoped/pure material, e.g. parent material of HTSCs, the resistivity of the material is given already by a single crystal unit cell. If the material is doped the resistivity changes. This is a very strong effect, because for HTSC materials the undoped/pure parent material is in many cases

an insulator and by doping it turns into a conducting material with a typical value of $\rho = \sim 10^{-6}$ Ω m. The smallest volume unit, which represents the resistivity of the doped material, is for HTSCs the superconducting unit volume V_{SC} for optimum doping (Fig. 1a).

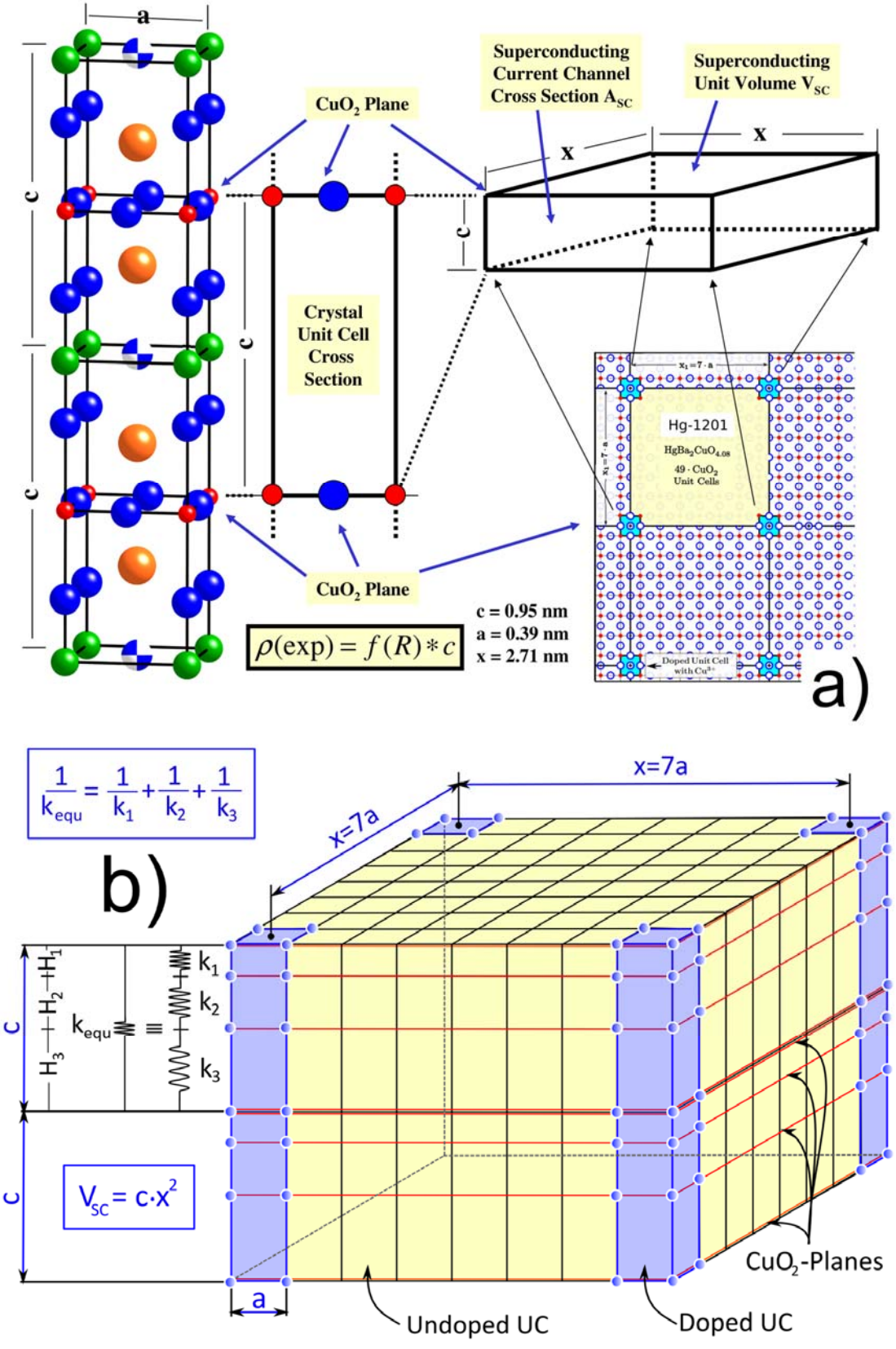

Fig. 1. Unit cell, cross section and superconducting unit volume of HTSC materials: a) single-mode Hg-1201 with 1 CuO_2 plane and b) arbitrarily chosen multimode structure with 3 CuO_2 planes.

Above T_c all HTSC materials behave like a classical device. Therefore, in view of Fig. 1a and equations (1, 2) different HTSC materials will be analysed by plotting the experimental resistivity value ρ(exp) at $\sim T_c$ versus the geometry parameter A_{SC}/L_{SC} of the superconducting unit volume. According to equation (2) the proportionality factor has the dimension [Ω] and therefore is a function of resistance $f(R)$ leading to

$$\rho(\exp) = f(R)\frac{A_{SC}}{L_{SC}} = f(R)\frac{W_{SC}H}{L_{SC}}. \qquad (4)$$

For the material Hg-1201 the ratio $A_{SC}/L_{SC} = c$ is given by the distance between the CuO_2 planes. This means that the resistivity is determined by the closest neighbor of superconducting carriers, because the distance between CuO_2 planes in c-direction is mostly much smaller than the doping distance x longwise and crosswise (Fig. 1a). Additionally, measuring the resistivity at $\sim T_c$ and knowing the doping/charge density per chemical formula it is also possible to estimate the mean time τ between collisions of superconducting carriers and their mobility μ.

4. Selection Procedure for resistivity-temperature curves

Figures 2–4 show 10 different examples for ρ-*T*-curves of HTSC materials (cuprates), which have been experimentally determined by many authors and are representative for typical curves. The selected HTSCs are covering a transition temperature range $\sim 20\ \mathrm{K} < T_c < \sim 135\ \mathrm{K}$ and a resistivity range $(\sim 0.5 < \rho(\exp) < \sim 1.5) \times 10^{-6}$ Ω m. For the following analysis T_c is considered to be taken at half of the transition interval of the resistivity-temperature curves in contrast to the onset transition temperature often used in literature. The experimental resistivity at T_c has been determined by the intersection of the T_c-ordinate and the extrapolation of the ρ-*T*-curve predominately below 200 K.

HTSC materials show a strong anisotropy in resistivity. Therefore ρ-*T*-curves in CuO_2-plane of single crystals have been used for this investigation. In c-axis – vertical to the CuO_2 plane – the resistivity is many times higher.

Optimum doping is mostly referred to maximum transition temperature. Therefore ρ-*T*-curves of different authors at optimum doping and/or curves slightly above or below optimum doping have been chosen for estimating the uncertainty of resistivity values at $\sim T_c$. In many cases it is well documented that overdoping as well as underdoping reduces the maximum T_c value [2]. Figures 3a, 3b, 4b and 4c are very good examples for this statement.

The following analysis does not consider very thin HTSC-films, because the resistivity could be strongly affected and reduced by a factor 10–100 when grown on different substrates.

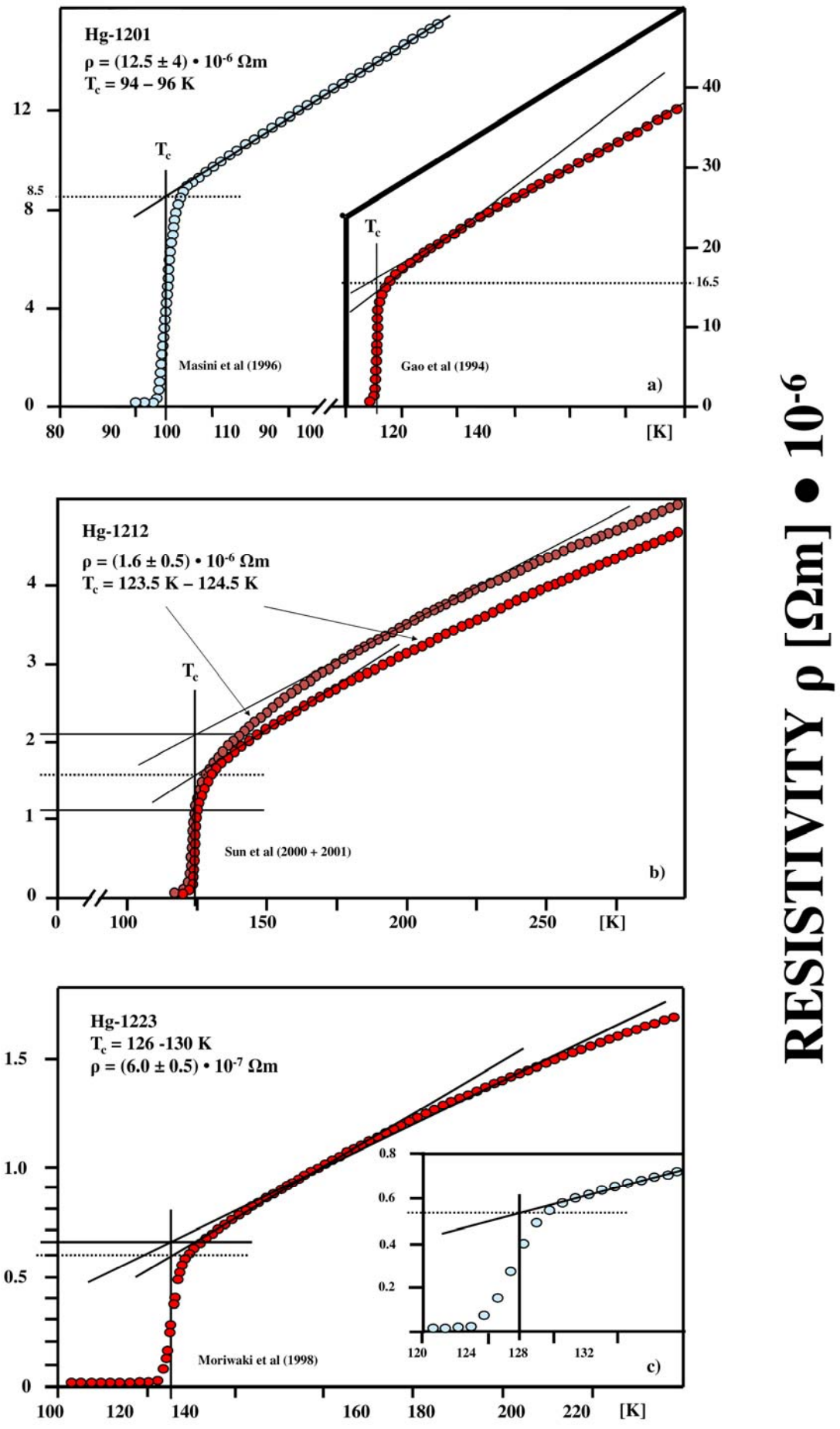

Fig. 2. Experimental resistivity ρ(exp) versus temperature curves for different HTSC materials from different authors: a) Hg-1201 [3,4], b) Hg-1212 [7,8] and c) Hg-1223 [9].

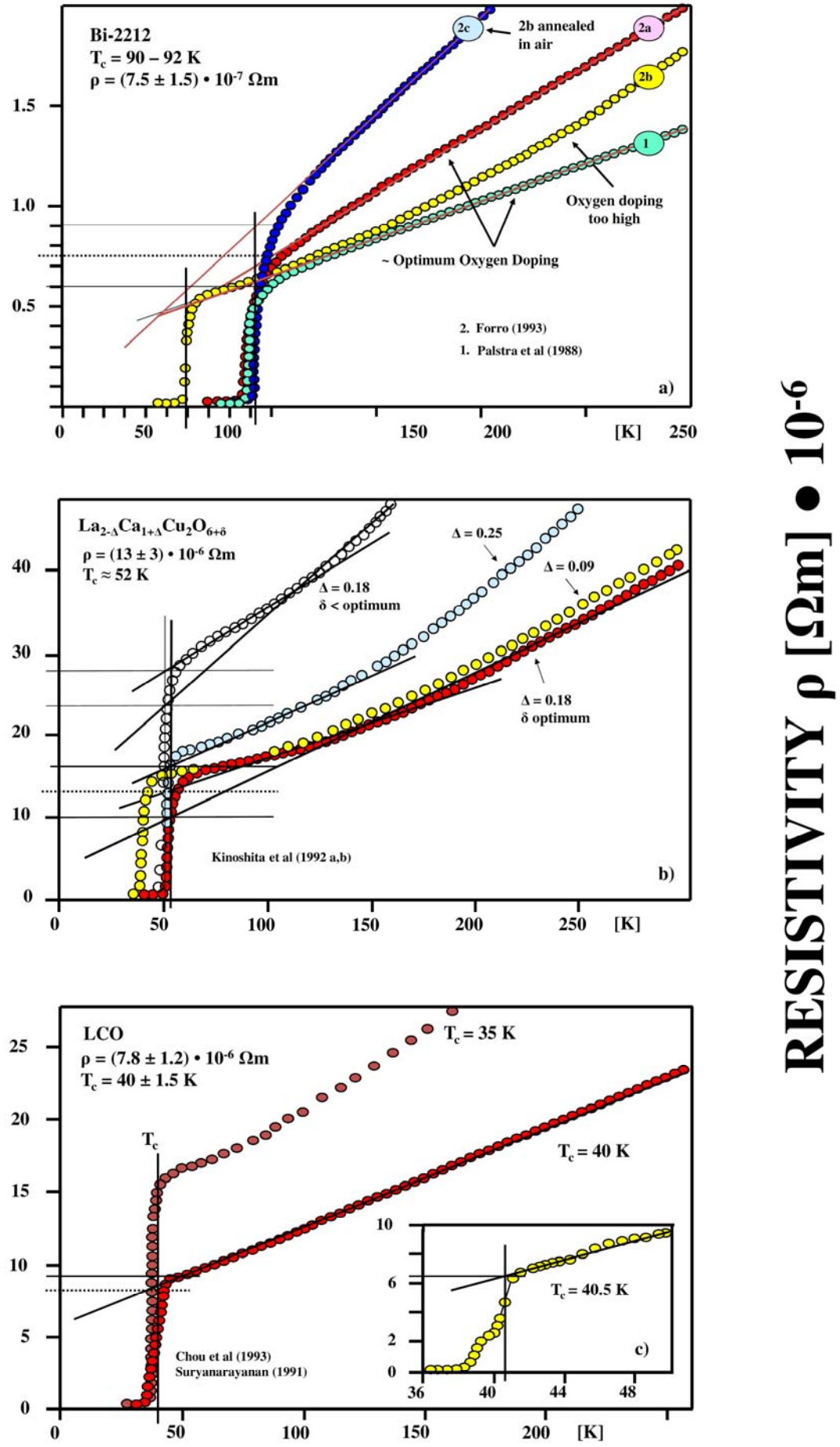

Fig. 3. Experimental resistivity ρ(exp) versus temperature curves for different HTSC materials from different authors: a) Bi-2212 [21,22,23], b) LCCO [26,31] and c) LCO [35,36].

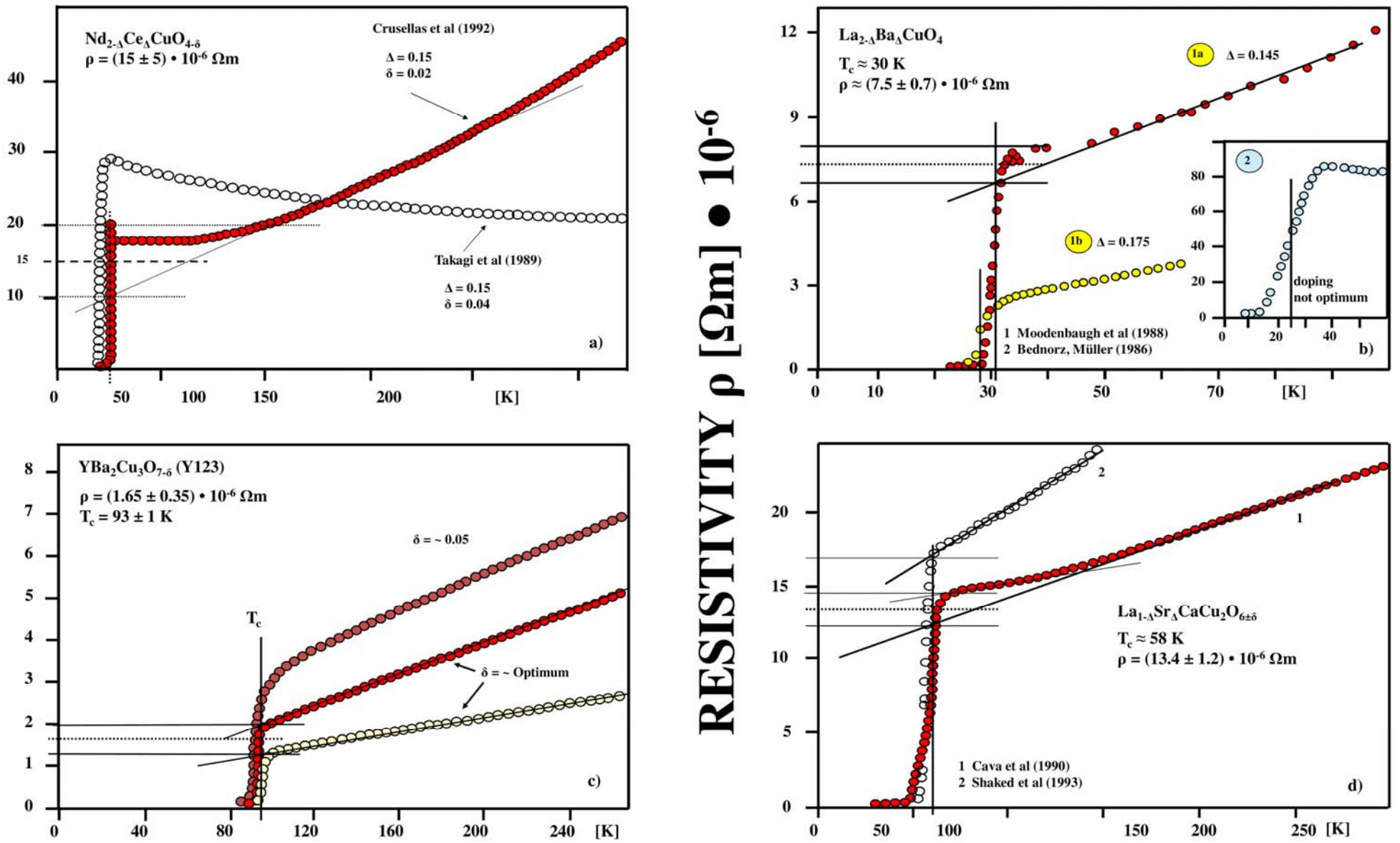

Fig. 4. Experimental resistivity ρ(exp) versus temperature curves for different HTSC materials from different authors: a) NCCO [2,18], b) LBCO [37,38,39], c) Y123 from e.g. Nobel lecture note by Bednorz [39] and d) LSCCO [32, 33].

5. Hg-1201

Figure 1a shows the HTSC material Hg-1201 and its superconducting CuO_2 plane with a squared doping distribution [1]. The tetragonal crystal structure has only one CuO_2 plane per crystal unit cell ($n_l = 1$). The next CuO_2 planes belong to the neighboring Hg-1201 monolayers above or below and are separated by the lattice constant *c*. A superconducting channel of width W_{SC} and height *H* has a cross section of $A_{SC} = xc = 2.58\times10^{-18}$ m^2 assuming to form a bundle of parallel current channels throughout the whole crystal.

The superconducting unit volume of $V_{SC} = x^2c = 6.98\times10^{-27}$ m^3 leads to a doping density of $N_D = 1.43\times10^{26}$ m^{-3} and a charge density of $2N_D = N_e = 2.86\times10^{26}$ m^{-3}. Using equation (3) the mean time between carrier collisions at $\sim T_c$ and their mobility can be calculated to $\tau(T_c) \approx 1.0\times10^{-14}$ s and $\mu(T_c) \approx 1.75\times10^{-3}$ m^2 V^{-1} s^{-1}.

Figure 2a shows the experimental ρ-*T*-curves for two detailed investigations [3,4]. The analysis results in $\rho(\text{exp}) = (12.5\pm4)\times10^{-6}$ Ω m. In Figs. 2–4 the error bars are in general determined by the nonlinearity of the curve above T_c, the sharpness of the transition, the deviation from the real optimum doping level, and the systematic errors of the experimental set-up by different authors.

According to equation (4) and $A_{SC}/L_{SC} = c = 0.950$ nm it results in a resistance of $f(R) = \rho(\text{exp})/c = (13.2\pm4)\times10^3$ Ω. This value is very close to the fundamental resistance of a single-mode ballistic conductor

$$R_{sm} = h/2e^2 \approx 12,906\ \Omega, \tag{5}$$

when size quantization plays a dominant role [5,6]. The contact resistance of a single-mode conductor is the resistance of a ballistic waveguide, which is independent of its length. The current channel in figure 1a looks very much like a waveguide. For a multimode ballistic conductor with $N_{mode} = 2,3,\ldots$ the contact resistance reads

$$R_{mm} = \frac{1}{N_{mode}}\frac{h}{2e^2}. \tag{6}$$

6. Resistivity and Multimode Conductors

In the previous section the resistance of a single-mode conductor with one superconducting plane per unit cell and one Cu^{3+}-ion per chemical formula has been considered. But multimode conductors are also possible. For cuprates this situation is given:

- if a doped unit cell has $n_1 = 2$ or more superconducting CuO_2 planes per chemical formula and/or
- if the doped unit cell consists of more than one chemical formula ($n_2 > 1$) on top of each other.

Following equation (6) with the idea of a multimode ballistic conductor, equation (4) has to be modified by several measures:

CuO_2 Planes and total Resistance

The total number of modes will be given by the total number of CuO_2 planes per unit cell

$$N_{\text{mode}} = n_1 \times n_2, \tag{7}$$

where n_1 is the number of CuO_2 planes per chemical formula and n_2 is the number of chemical formulas on top of each other per unit cell. At T_c superconducting carriers are moving coherently in phase along the CuO_2 plane. Therefore it is justified assuming that the resistance in each mode is the same so that the total resistance of N_{mode} parallel resistances per unit cell is given by $R_{tot} = f(R)/N_{\text{mode}}$.

Doping Density

According to equation (3) the resistivity depends also on the doping density of the carriers. For the Hg-series there exists only one Cu^{3+}-ion per chemical formula (Table 1) and so far the analysis is based on one Cu^{3+}-ion per superconducting unit volume. But as it will be shown later on, several HTSC materials contain two Cu^{3+}-ions per chemical formula. To account for $n_3 = 2$ or even more Cu^{3+}-ions per chemical formula we introduce

$$\rho \sim \frac{1}{n_3}. \tag{8}$$

Resistivity in Subchannels

For an undoped (pure) material the resistivity is determined already by the property of one single unit cell. For HTSCs with uniform doping the resistivity is given by a superconducting unit cell with volume V_{SC}. For an arbitrary example Fig. 1b illustrates qualitatively this situation for a squared doping distribution. The doped unit cell crystals are at the corners, and top and bottom are formed by CuO_2 planes separated by the lattice constant $H = c$. Additionally, Fig. 1b shows a three mode configuration with CuO_2 plane separations H_1, H_2 and H_3. As already pointed out in section 3 the resistivity is dominated by the coupling perpendicular to the current flow. Therefore the total resistivity of the superconducting unit volume is given by resistivities of the subvolumes as

illustrated in Fig. 1b. The resulting equivalent coupling k_{equ} for coupling values k_i in series in *c*-direction leads to

$$1/\rho_{\text{tot}} \sim \left(L_{SC}/W_{SC}\right)\sum_i \left(1/H_i\right) = 1/L_R \tag{9}$$

by introducing an effective resistivity length L_R for convenience.

Shifted Stacking Sequence

Several HTSC materials, like NCCO, Bi-2212 and LCO, consist of two chemical formulas on top of each other ($n_2 = 2$) and additionally with CuO_2 planes having a shifted stacking sequence (sections 10–14). The alternating CuO_2 planes are shifted by $a/2$ in both directions of the CuO_2 plane. Figure 5 illustrates the shifted stacking sequence for the HTSC material Bi-2212 (see also section 11). To contribute for this geometrical arrangement with $L_{SC} = W_{SC}$ only the coupling in c-direction has to be considered as parallel but equal coupling chains by introducing the relation

$$\rho \sim n_4, \tag{10}$$

where n_4 is the number of different shifted stacking sequences per unit cell.

For multimode ballistic conductors equation (4) needs to be modified considering equations (7–10) which leads to

$$\rho(\text{exp}) = \left(f(R)/N_{\text{mode}}\right)\left(n_4/n_3\right)L_R = \left(f(R)n_4/n_1n_2n_3\right)L_R. \tag{11}$$

In the following sections HTSC materials will be analyzed by plotting ρ(exp) at $\sim T_c$ versus $n_4L_R/N_{\text{mode}}n_3$ to find out if equation (11) has a universal meaning.

7. Hg-1212

Figure 6a shows the unit cell of HTSC material Hg-1212, which has two CuO_2 planes. Therefore the superconducting unit volume consists of two different sub-channels or two modes $N_{\text{mode}} = n_1 = 2$. It has one chemical formula per unit cell ($n_2 = 1$), one Cu^{3+}-ion per chemical formula (Table 1, 2) and $L_{SC} = W_{SC}$ which leads to

$$\rho(\text{exp}) = \left(f(R)/2\right)\left[H_1 \times H_2/\left(H_1 + H_2\right)\right] = f(R)\left(L_R/2\right). \tag{12}$$

Figure 2b illustrates the experimental results for two different samples with $T_c = 124.5$ K and 123.5 K respectively, which are very close to the maximum value of $T_c\left(\max\right) = 126 \pm 1.5$ K [7, 8]. The ρ-*T* curves, which do not show a sharp bend at T_c, suggest a value of $\rho\left(\exp\right) = \left(1.6 \pm 0.5\right)\times 10^{-6}$ Ω m. With the crystal structure values $c = 1.265$ nm, $H_1 = 0.325$ nm and $H_2 = 0.940$ nm the resistance results in $f\left(R\right) = \left(13.3 \pm 4.2\right)\times 10^3$ Ω.

Table 1. Chemical formulas of undoped and doped crystal structures of 10 different HTSC materials including their mode structure values: n_1 is the number of CuO_2 planes per chemical formula and n_2 is the number of chemical formulas on top of each other per unit cell; n_3 is the number of Cu^{3+}-ions per chemical formula and n_4 is the number of different shifted stacking sequences per unit cell.

Material	Undoped Chemical Formula / Crystal Structure	Doped Chemical Formula / Doping Structure		n_1	n_2	N_{mode}	n_3	n_4
$HgBa_2CuO_{4+\delta}$ Hg-1201	$Hg^{2+} + 2Ba^{2+} + Cu^{2+} + 4O^{2-}$ tetragonal	$Hg^{3+} + 2Ba^{2+} + Cu^{3+} + 5O^{2-}$ squared		1	1	1	1	1
$HgBa_2CaCu_2O_{6+\delta}$ Hg-1212	$Hg^{2+} + 2Ba^{2+} + Ca^{2+} + 2Cu^{2+} + 6O^{2-}$ tetragonal	$Hg^{3+} + 2Ba^{2+} + Ca^{2+} + Cu^{2+} + Cu^{3+} + 7O^{2-}$ squared		2	1	2	1	1
$HgBa_2Ca_2Cu_3O_{8+\delta}$ Hg-1223	$Hg^{2+} + 2Ba^{2+} + 2Ca^{2+} + 3Cu^{2+} + 8O^{2-}$ tetragonal	$Hg^{3+} + 2Ba^{2+} + 2Ca^{2+} + 2Cu^{2+} + Cu^{3+} + 8O^{2-}$ squared		3	1	3	1	1
$YBa_2Cu_3O_{7-\delta}$ Y123	$Y^{2+} + 2Ba^{2+} + 3Cu^{2+} + 6O^{2-}$ orthorhombic	$Y^{3+} + 2Ba^{2+} + 2Cu^{2+} + Cu^{3+} + 7O^{2-}$ squared		2	1	2	1	1
$Nd_{2-\Delta}Ce_{\Delta}CuO_{4-\delta}$ NCCO	$2Nd^{3+} + Cu^{2+} + 4O^{2-}$ tetragonal	$Nd^{3+} + Ce^{4+} + Cu^{1+} + 2e^{-} + 3O^{2-}$ squared		1	2	2	1	2
$La_{2-\Delta}Ca_{1+\Delta}Cu_2O_{6+\delta}$ LCCO	$2La^{3+} + Ca^{2+} + 2Cu^{2+} + 6O^{2-}$ tetragonal	squared	$2La^{3+} + Ca^{2+} + 2Cu^{3+} + 7O^{2-}$	2	1	2	2	2
			$3Ca^{2+} + 2Cu^{3+} + 6O^{2-}$	2	1	2	2	2
$La_{2-\Delta}Sr_{\Delta}CaCu_2O_{6+\delta}$ LSCCO	$2La^{3+} + Ca^{2+} + 2Cu^{2+} + 6O^{2-}$ tetragonal	squared	$2La^{3+} + Ca^{2+} + 2Cu^{3+} + 7O^{2-}$	2	1	2	2	2
			$3Sr^{2+} + 2Cu^{3+} + 6O^{2-}$	2	1	2	2	2
$Bi_2Sr_2CaCu_2O_{8+\delta}$ Bi-2212	$2Bi^{3+} + 2Sr^{2+} + Ca^{2+} + 2Cu^{2+} + 8O^{2-}$ orthorhombic	$2Bi^{3+} + 2Sr^{2+} + Ca^{2+} + 2Cu^{3+} + 9O^{2-}$ squared		2	2	4	2	2
$La_2CuO_{4+\delta}$ LCO	$2La^{3+} + Cu^{2+} + 4O^{2-}$ orthorhombic	$4La^{3+} + 2Cu^{3+} + 9O^{2-}$ regular triangle		1	2	2	2	2
$La_{2-\Delta}Ba_{\Delta}CuO_4$ LBCO	$2La^{3+} + Cu^{2+} + 4O^{2-}$ orthorhombic	$2La^{3+} + 2Ba^{2+} + 2Cu^{3+} + 8O^{2-}$ regular triangle		1	2	2	2	2

Table 2. Investigation of mode and crystal structure in combination with experimental resistivity at the transition temperature for 10 prominent HTSCs.

Material	Crystal Structure [nm]	T_c [K] (exp)	N_{mode}	n_3	n_4	$\rho = \frac{f(R)}{N_{mode}} \frac{n_4}{n_3} L_R$	$\frac{L_R}{N_{mode}} \frac{n_4}{n_3}$ [10^{-10} m]	Resistivity $\rho(exp)$ [10^{-6} Ωm]	Resistance $f(R)$ [10^3 Ω]
$HgBa_2CuO_{4+\delta}$ Hg-1201	a = 0.388 c = 0.950	95 ± 1	1	1	1	$f(R)*c$	9.50	12.5 ± 4	13.2 ± 4
$HgBa_2CaCu_2O_{6+\delta}$ Hg-1212	a = 0.386 c = 1.265	126 ± 1.5	2	1	1	$\frac{f(R)}{2}\left[\frac{H_1H_2}{c}\right]$	1.21	1.6 ± 0.5	13.3 ± 4.2
$HgBa_2Ca_2Cu_3O_{8+\delta}$ Hg-1223	a = 0.385 c = 1.610	134 ± 2	3	1	1	$\frac{f(R)}{3}\left[\frac{H_1H_3}{2H_3+H_1}\right]$	0.462	0.6 ± 0.05	13.0 ± 1.1
$YBa_2Cu_3O_{7-\delta}$ Y123	a = 0.39 c = 1.17	93 ± 1	2	1	1	$\frac{f(R)}{2}\left[\frac{H_1H_2}{c}\right]$	1.32	1.65 ± 0.35	12.7 ± 2.7
$Nd_{2-\Delta}Ce_{\Delta}CuO_{4-\delta}$ NCCO	a = 0.394 c = 1.207	22 ± 1	2	1	2	$f(R)*c$	12.1	15 ± 5	12.4 ± 4.1
$La_{2-\Delta}Ca_{1+\Delta}Cu_2O_{6+\delta}$ LCCO	a = 0.383 c = 1.945	52.5 ± 1	2	2	2	$f(R)*\frac{c}{2}$	9.72	13 ± 3	13.4 ± 3.1
$La_{2-\Delta}Sr_{\Delta}CaCu_2O_{6+\delta}$ LSCCO	a = 0.382 c = 1.960	58 ± 1	2	2	2	$f(R)*\frac{c}{2}$	9.80	13.4 ± 1.2	13.6 ± 1.2
$Bi_2Sr_2CaCu_2O_{8+\delta}$ Bi-2212	a = 0.38 c = 3.08	91 ± 1	4	2	2	$\frac{f(R)}{4}\left[\frac{H_1H_2}{c}\right]$	0.59	0.75 ± 0.15	12.75 ± 2.6
$La_2CuO_{4+\delta}$ LCO	a = 0.38 c = 1.32	40 ± 1.5	2	2	2	$f(R)*\frac{c}{2}\sqrt{\frac{3}{4}}$	5.7	7.8 ± 1.2	13.6 ± 2.1
$La_{2-\Delta}Ba_{\Delta}CuO_4$ LBCO	a = 0.38 c = 1.32	30 ± 1	2	2	2	$f(R)*\frac{c}{2}\sqrt{\frac{3}{4}}$	5.7	7.5 ± 0.7	13.1 ± 1.2

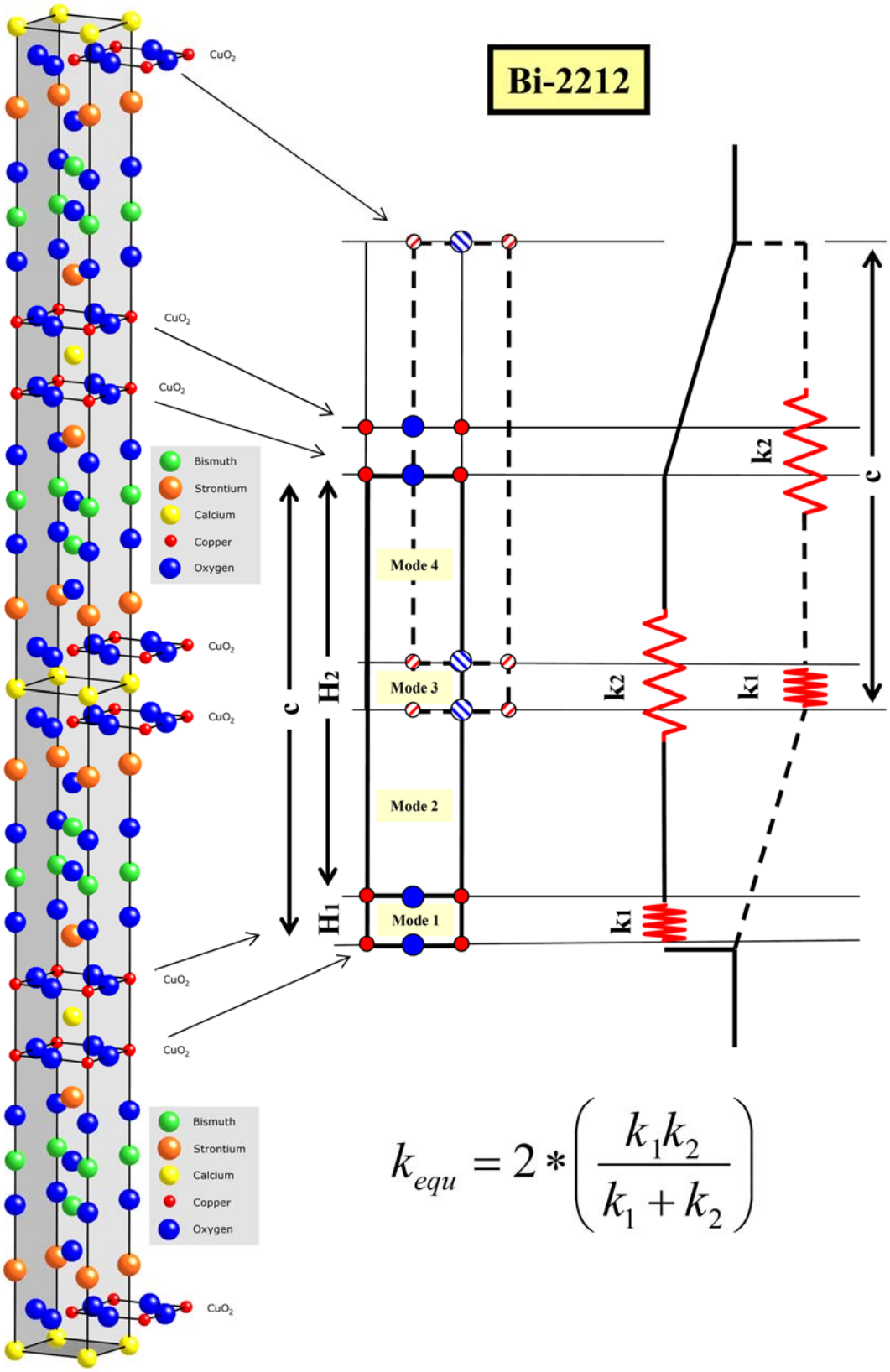

Fig. 5. Unit cell and cross section of the multimode HTSC material Bi-2212 with shifted stacking sequence.

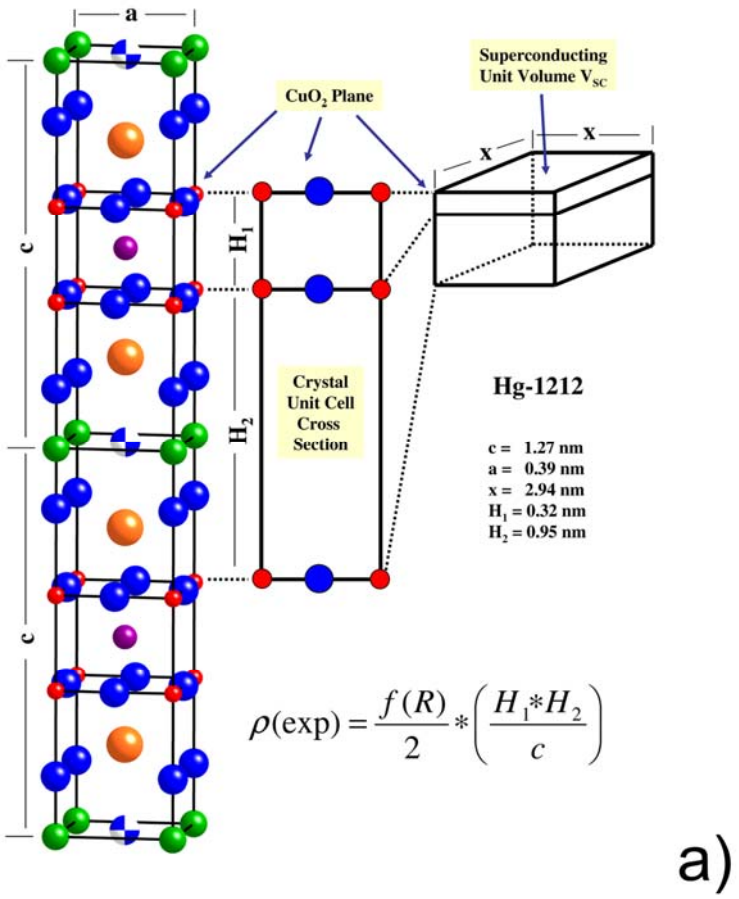

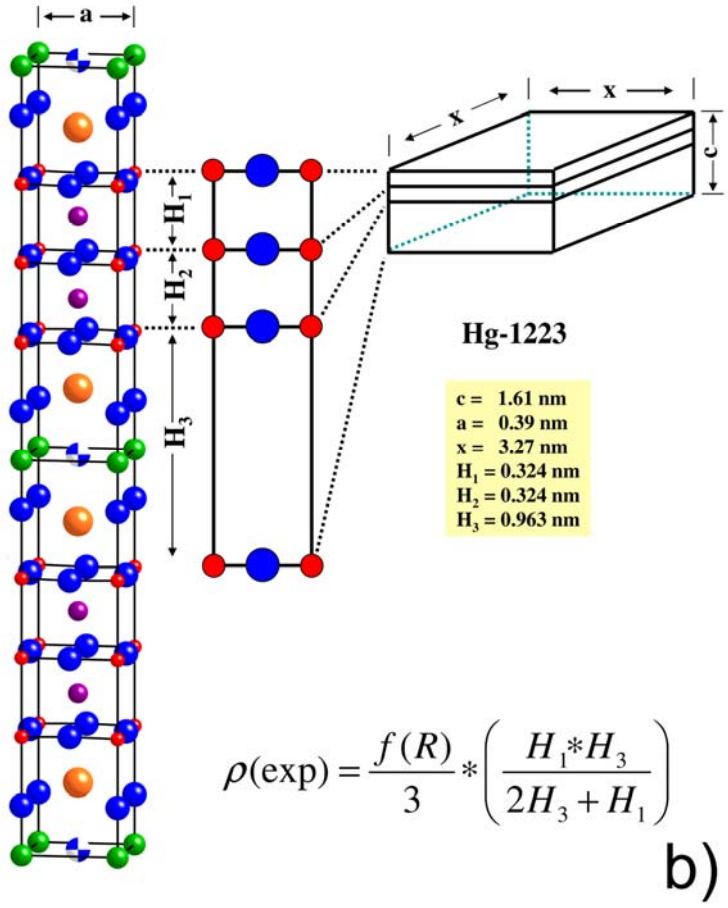

Fig. 6. Unit cell, cross section and superconducting unit volume of HTSC materials: a) 2-mode Hg-1212 with 2 CuO_2 planes and b) 3-mode Hg-1223 with 3 CuO_2 planes.

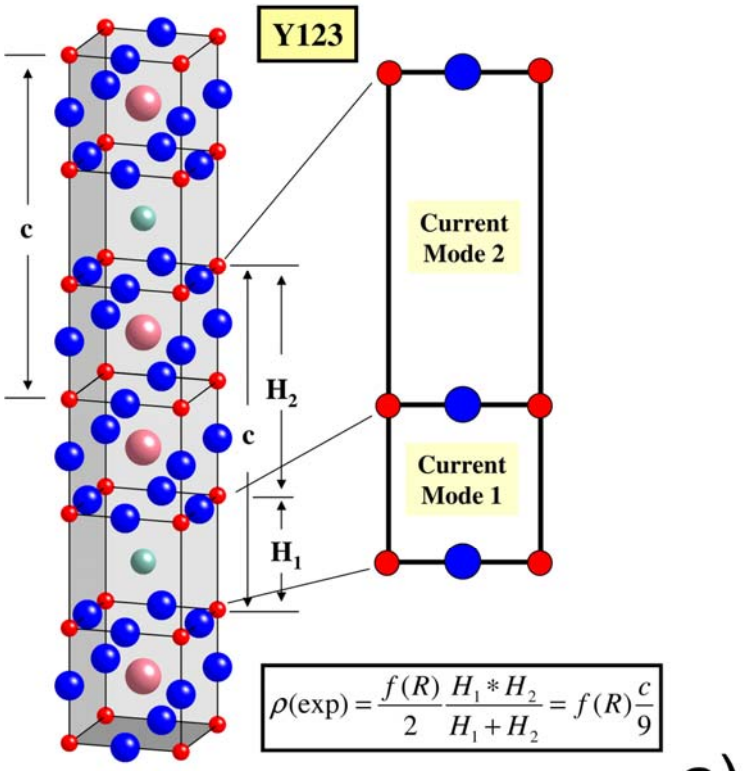

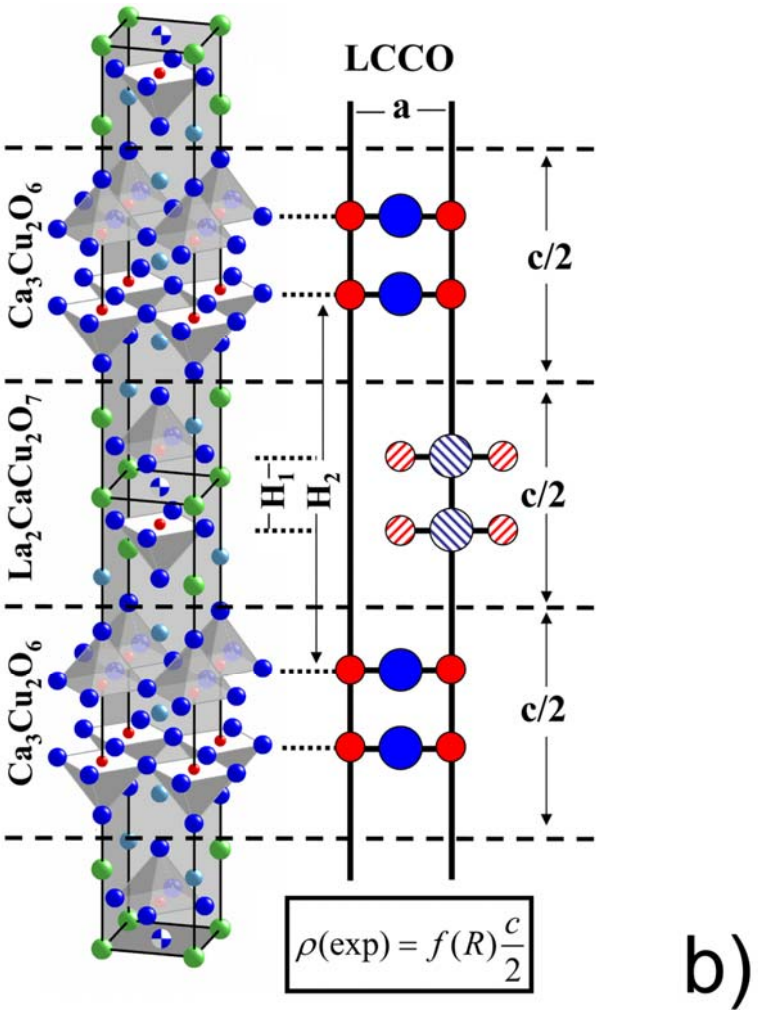

Fig. 7. Unit cell, cross section and superconducting unit volume of HTSC materials: a) 2-mode Y123 with 2 CuO_2 planes and b) LCCO consisting of two different HTSC materials.

8. Hg-1223

The unit cell of the crystal contains $n_1 = 3$ CuO_2 planes and therefore has $N_{\text{mode}} = 3$ modes. The superconducting unit volume is made up of 3 sub-volumes which differ only in height (Fig. 6b). Figure 1b is schematically equivalent to Fig. 6b. Using equations (9,11) and $H_1 = H_2$ the effective resistivity length can be calculated by

$$1/L_R = \left(1/H_1 + 1/H_2 + 1/H_3\right) = \left(2H_3 + H_1\right)/H_1H_3 \tag{13}$$

with $H_1 = 0.324$ nm and $H_3 = 0.963$ nm it leads to the total resistivity:

$$\rho_{\text{tot}} = \frac{f(R)}{3}\frac{H_1H_3}{2H_3 + H_1} = f(R)\frac{L_R}{3}. \tag{14}$$

The experimental ρ-*T*-curves [9] in Fig. 2c suggest a value of $\rho(\text{exp}) = (6.0 \pm 0.5)\times 10^{-7}$ Ω m. With $L_R/3 = 4.62\times 10^{-11}$ m it leads to $f\left(R\right) = \left(13.0 \pm 1.1\right)\times 10^3$ Ω.

9. Y-123

The Y-123 HTSC material $Y_1Ba_2Cu_3O_{7-\delta}$ is one of the best known and most widely used HTSC. It has a fully ordered orthorhombic crystal lattice (Fig. 7a) compared to the similar but tetragonal structure of Hg-1212. The doping distribution is squared, so that equation (12) can be used too. The crystal parameters are $a \approx b \approx 0.39$ nm, $c = 1.17$ nm, $H_1 = c/3$ and $H_2 \approx 2c/3$ with $c = H_1 + H_2$ resulting in $\rho(\text{exp}) = f\left(R\right)\times c/9$. The experimental resistivity (Fig. 4c) of $\rho(\text{exp}) = (1.65 \pm 0.35)\times 10^{-6}$ Ω m results in $f\left(R\right) = \left(12.7 \pm 2.7\right)\times 10^3$ Ω [10-13]. It is worth noticing that the resistivity can be as high as ~30×10^{-6} Ω m if the doping is not optimized to δ ≈ 0.04 or additional dopants (e.g. Pt, Au) and Y211 impurity phase transitions are present. Additionally, very thin film devices as well as high pressure reduce the resistivity down to values as low as $(0.5–0.8)\times 10^{-6}$ Ω m [14-17].

10. NCCO

The HTSC material $Nd_{2-\Delta}Ce_{\Delta}CuO_{4-\delta}$ is an electron doped (N-type) superconductor with an excess of $2e^-$ in the doped chemical formula (Table 1) and a transition temperature of about $T_c \approx 22$ K. It has a so-called tetragonal T'-phase crystal structure (Fig. 8a) with no apical O-atom above and/or below the CuO_2-plane. The parameters of the unit cell are $a = 0.394$ nm and $c = 1.207$ nm and it consists of $n_2 = 2$ chemical formulas on top of each other. Therefore the number of parallel modes per unit cell is now given by $N_{\text{mode}} = n_1 \times n_2 = 2$. In comparison to Hg-1201 the CuO_2 plane in the middle is shifted by $a/2$ in both directions of the CuO_2 plane.

Therefore it yields $n_4 = 2$. Detailed resistivity measurements have been made in large single crystals with a bulk size of 2.2×3.2×0.2 mm^3 in the CuO_2 plane [18], and additionally in *c*-direction by CuO_2 layered compounds [2]. Figure 4a illustrates both resistivity-temperature curves. The highest transition temperature is achieved with $\delta = 0.02$ and $\Delta = 0.15$ [18,19] whereas with $\delta = 0.04$ and $\Delta = 0.15$ [2] the curve is different having a lower T_c. The experimental resistivity results in $\rho(\text{exp}) = (15 \pm 5) \times 10^{-6}$ Ω m in contrast to ~6×10^{-3} Ω m in *c*-direction. If very thin NCCO films are used, which are grown on special substrates, the resistivity is reduced typically down to ~1×10^{-7} Ω m [20]. Equation (11) leads to $f(R) = (12.4 \pm 4.1) \times 10^3$ Ω.

11. Bi-2212

The unit cell of Bi-2212 is illustrated in Fig. 5. It consists of two chemical formulas on top of each other ($n_2 = 2$) with pairs of CuO_2 planes ($n_1 = 2$) having a shifted stacking sequence ($n_4 = 2$). Bi-2212 has $N_{\text{mode}} = n_1 \times n_2 = 4$ modes given by four CuO_2 planes. Table 1 illustrates that for HTSCs in previous sections there was only one Cu^{3+}-ion per chemical formula available. But instead the chemical formula of Bi-2212 offers two Cu^{3+}-ions ($n_3 = 2$). With equation (11) this leads to $\rho(\text{exp}) = f(R) \times 5.9 \times 10^{-11}$ m. With the experimental value $\rho(\text{exp}) = (7.5 \pm 1.5) \times 10^{-7}$ Ω m illustrated in Fig. 3a [21, 22, 23] and with $c = 3.08$ cm $= H_1 + H_2$ and $H_1 = c/12$, $H_1 = (11/12) \times c$ the resistance results in $f(R) = (12.75 \pm 2.6) \times 10^3$ Ω. In Fig. 3a curves 1 and 2a are taken for optimum doping, whereas curve 2b the doping is too high and for curve 2c the doping is too low.

12. LCCO and LSCCO

The compound $La_2CaCu_2O_6$ can be made superconducting by doping with Ca or Sr and by synthesis under high O_2 pressure in the form of $La_{2-\Delta}(Sr,Ca)_\Delta CaCu_2O_{6\pm\delta}$ [24, 25]. But it is possible to prepare an isomorphous material containing no Sr-atoms [26]. The double doped unit cell of $La_{2-\Delta}Ca_{1+\Delta}Cu_2O_{6+\delta}$ (LCCO) has a simple tetragonal crystal structure (Fig. 7b) and the unit cell ($a = 0.383$ nm, $c = 1.945$ nm) consists of 2×($La_{2-\Delta}Ca_{1+\Delta}Cu_2O_{6+\delta}$). This HTSC does not change its crystal structure when cooling down to low temperatures [27,28]. The double doped unit cell consists of two different chemical formulas, $La_2CaCu_2O_7$ and $Ca_3Cu_2O_6$ which are responsible for the occurrence of superconductivity at about $T_c = 52$ K with $n_1 = 2$ superconducting CuO_2 planes per chemical formula [29,30]. But the O-doped and Ca-doped elements have to be considered as two different and alternating HTSC materials with 2Cu^{3+}-ions per chemical formula each (Table 1). Therefore the parameters are $n_1 = 2$, $n_2 = 1$, $n_3 = 2$, and $n_4 = 2$. According to equation (11) this

leads to $\rho(\text{exp}) = f(R)\times(c/2)$. Figure 3b shows several ρ-*T*-curves with different doping parameters. An estimate for the resistivity is $(13.3\pm3)\times10^{-6}$ Ω m, which results in $f(R) = (13.4\pm3.1)\times10^{3}$ Ω.

The HTSC material $La_{2-\Delta}Sr_{\Delta}CaCu_2O_{6\pm\delta}$ has an identical structure to LCCO with slightly different crystal parameters $a = 0.382$ nm and $c = 1.960$ nm. Replacing in LCCO some La-atoms by Sr-atoms increases the transition temperature by about 10%. As for LCCO we have the same situation of two independent HTSC layers with height $c/2$ each. The double doped unit cell consists of two different chemical formulas, $La_2CaCu_2O_7$ and $Sr_3Cu_2O_6$. The idea of considering different chemical formulas in one unit cell has already been suggested for

$La_{2-\Delta}Sr_{\Delta}CaCu_2O_{6+\delta}$ by Ulrich et al [29]. Therefore equation (11) should read $\rho(\text{exp}) = f(R)\times9.80\times10^{-10}$ Ω m. Detailed investigations demonstrated that optimum doping leads to a transition temperature of 58 K [31]. The ρ-*T*-curve (Fig. 4d) shows the curve for maximum T_c [32] and a curve slightly below T_c with a somewhat higher resistivity [33]. The estimate of the resistivity is $\rho(\text{exp}) = (13.4\pm1.2)\times10^{-6}$ Ω m which results in $f(R) = (13.6\pm1.2)\times10^{3}$ Ω.

13. LCO

So far, HTSC materials in sections 2–12 have a squared doping pattern as illustrated for example in Fig. 1a. But several HTSC materials, like $La_2CuO_{4.08}$ (LCO) with oxygen excess, show a different superconducting area in the CuO_2 plane which is formed by regular triangles [34]. Figure 8b illustrates that LCO is build up by neighboring rectangular current channels with cross section $A_{SC} = c\sqrt{0.75}x$ and length $L_{SC} = x$, so that $A_{SC}/L_{SC} \approx 0.866c$.

In one chemical formula [La_2CuO_4] four O-atoms ($4O^{2-}$) need in total eight electrons which are provided by $2La^{3+} + 1Cu^{2+}$. This material has no Cu^{3+}-elements and is not superconducting unless it is doped by an appropriate oxygen excess level. A small amount of interstitial oxygen between the copper-oxygen planes is responsible for the occurrence of superconductivity. At low temperatures the tetragonal unit cell transforms into an orthorhombic unit cell which then consists of $4\times(La_2CuO_{4+\delta})$ with two chemical formulas on top of each other ($n_2 = 2$). This means that one unit cell can host/accommodate two O-atoms where each O-atom connects with two chemical formulas $2\times(La_2CuO_{4+\delta})$ forming a chemical arrangement of $4La^{3+} + 2Cu^{2+} + 9O^{2-}$. The cross section of the doped unit cell consists of $2\times(CuO_2)$ elements and one excess O-atom transforms $2Cu^{2+}$ into $2Cu^{3+}$-ions (Fig. 9). In comparison with NCCO the material LCO is also considered as a

2-mode superconductor ($n_1 = 2$) because of the two CuO_2 planes. Additionally, the shifted stacking sequence has to be taken into account with $n_4 = 2.$ Therefore equation (11) leads to

$$\rho(\exp) = \frac{f(R) \times 2}{1 \times 2 \times 2} \sqrt{\frac{3}{4}} c = f(R) \frac{\sqrt{3} c}{4}. \tag{15}$$

Figure 3c illustrates the results of ρ-*T*-curves for several LCO materials with different T_c values [35, 36] leading to a resistivity of $\rho(\exp) = (7.8 \pm 1.2) \times 10^{-6}$ Ω m. The resistance results in $f(R) = 13.6 \times 10^3$ Ω.

14. LBCO

The HTSC material $La_{2-\Delta}Ba_{\Delta}CuO_4$ has the same crystal structure as LCO and shows the same behavior. Therefore equation (15) has to be applied leading to $\rho(\exp) = f(R) \times 6.60 \times 10^{-10}$ Ω m.

Figure 4b illustrates the results of ρ-*T*-curves for several LBCO materials with different T_c values [37,38,39] leading to a resistivity at maximum T_c of $\rho(\exp) = (7.5 \pm 0.7) \times 10^{-6}$ Ω m and the resistance results in $f(R) = 13.1 \times 10^3$ Ω.

15. Conclusion

Tables 1 and 2 summarize the different aspects of ten prominent HTSCs, which have been investigated. It is worth noticing that the investigation has only been done for $N_{\text{mode}} \leq 4$ modes, because to our knowledge there are no resistivity-temperature curves available for crystals with pure single phases with $n_1 \geq 4$ CuO_2 planes per unit cell and with or without shifted stacking sequences.

Figure 10 lists the ionization energies of the different atoms which are involved in the chemical arrangement for the doped chemical formulas summarized in Table 1. In Fig. 11 the experimental resistivity $\rho(\exp)$ of each HTSC is plotted versus $n_4 L_R / N_{\text{mode}} n_3$. In most cases there is a ratio of $n_4 / n_3 = 1$ except for NCCO. The data can be fitted by a straight line to

$$\rho(\exp) = m_3 \times \frac{L_R n_4}{N_{\text{mode}} n_3} - \rho_0, \tag{16}$$

where the slope m_3 has the value $m_3 = (13.39 \pm 0.79) \times 10^3$ Ω and $\rho_0 = (0.02 \pm 0.06) \times 10^{-6}$ Ω m. For further consideration ρ_0 will be neglected. Obviously the concept of multimode ballistic conductors works out fine, so that the slope m_3 could represent the fundamental resistance of a single-mode ballistic waveguide with $R = m_3 \approx h/2e^2$ as pointed out in section 5.

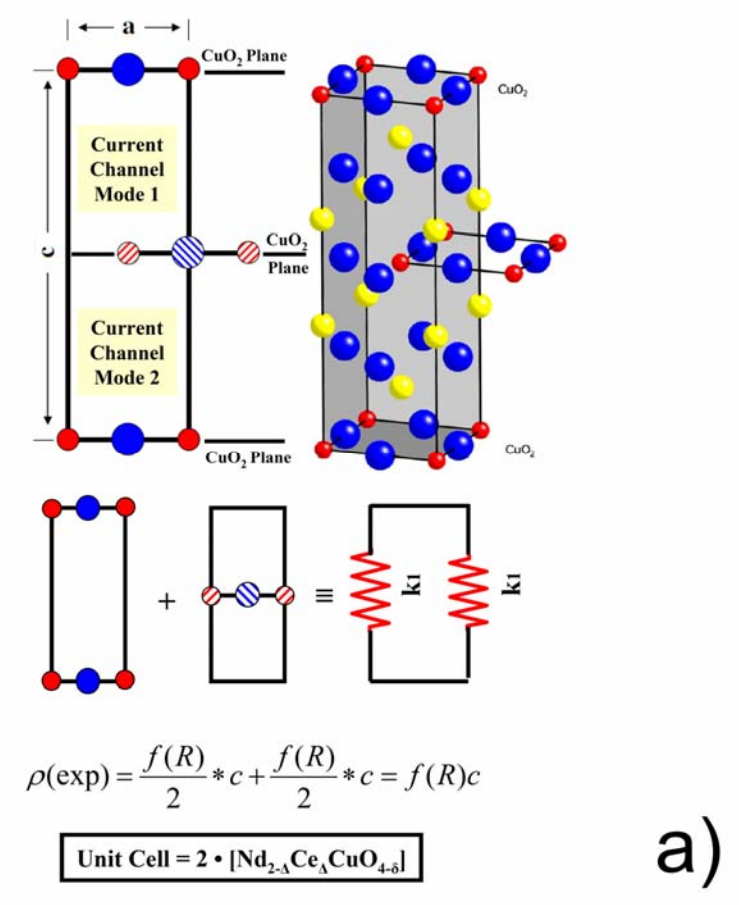

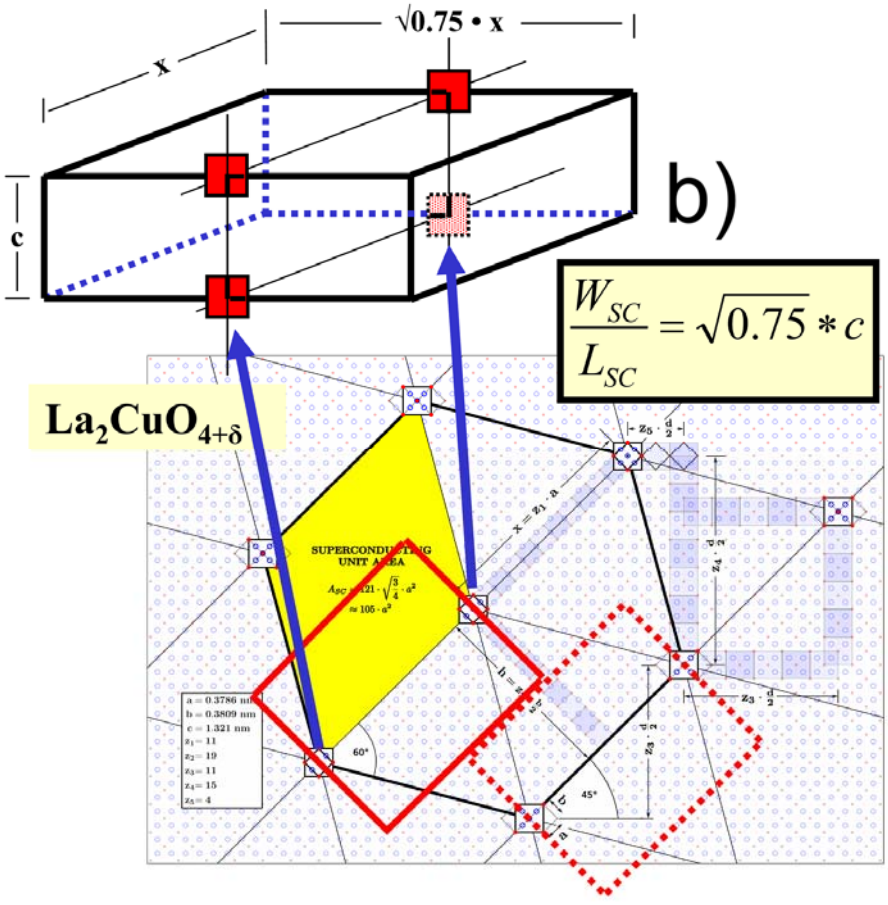

Fig. 8. a) Unit cell and cross section of the HTSC material NCCO with 2 modes and shifted stacking sequence and b) doping distribution and superconducting unit volume of LCO.

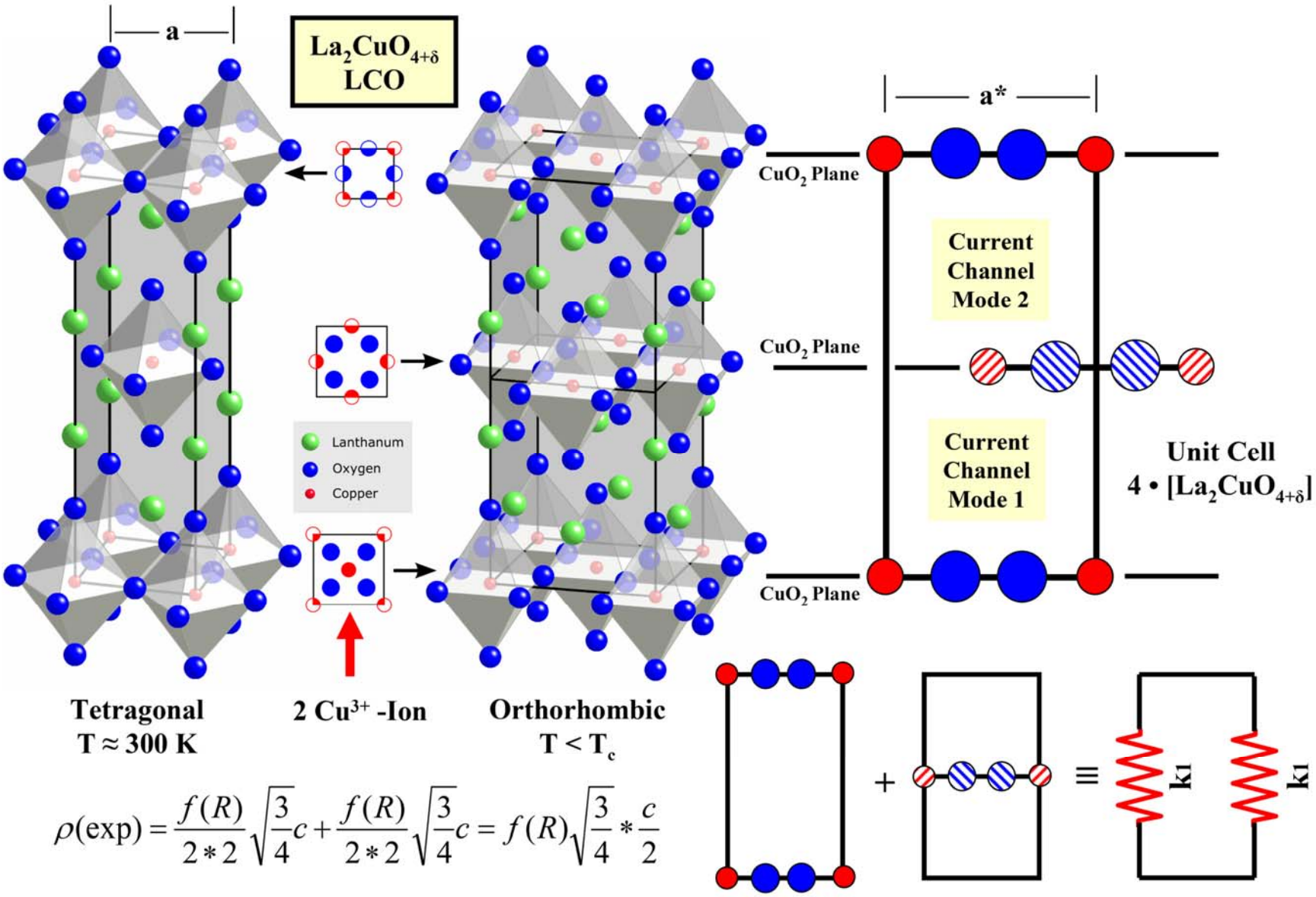

Fig. 9. Unit cell transformation of LCO when cooling down from ambient temperature to superconducting temperature.

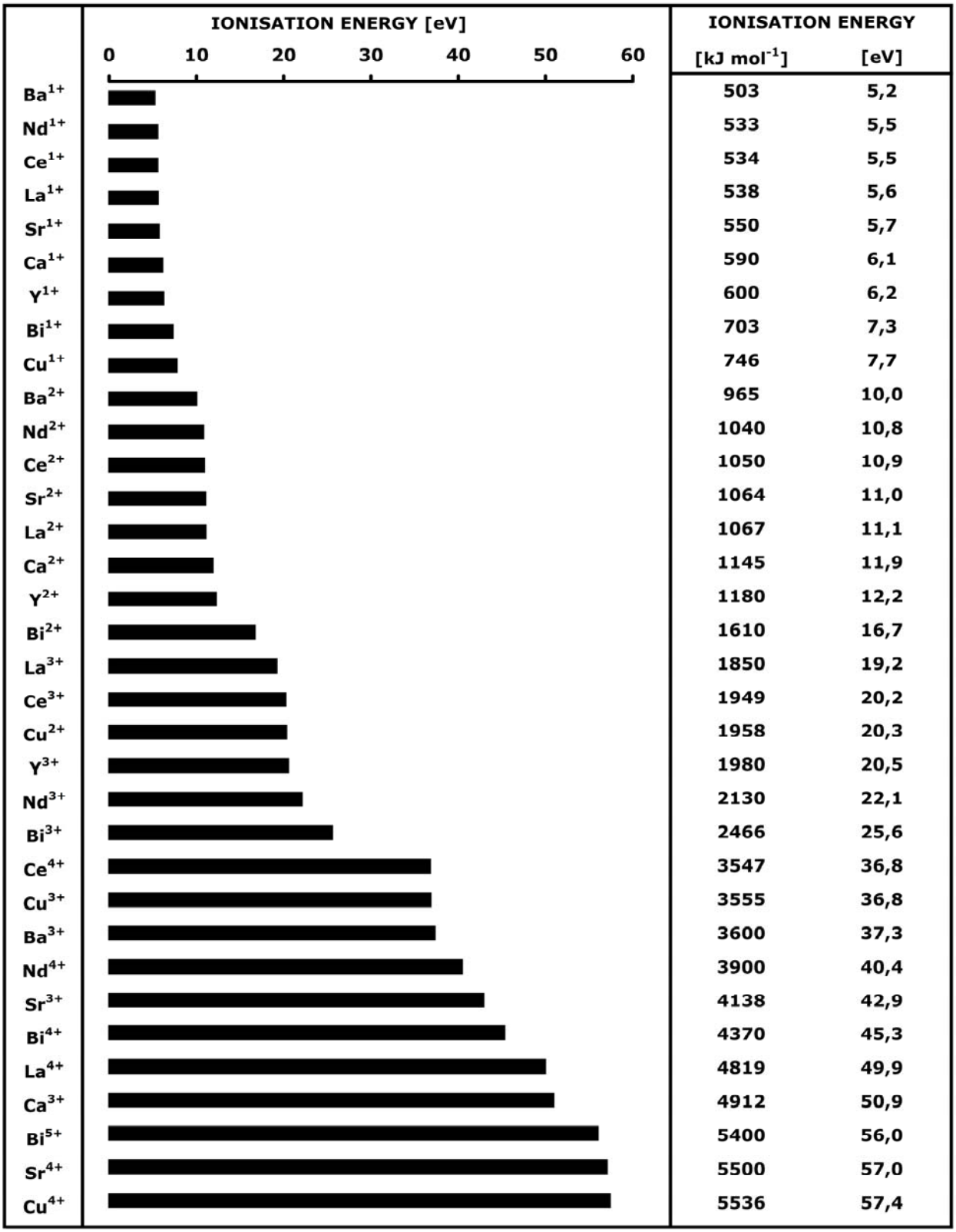

	IONISATION ENERGY [kJ mol^{-1}]	IONISATION ENERGY [eV]
Ba^{1+}	503	5,2
Nd^{1+}	533	5,5
Ce^{1+}	534	5,5
La^{1+}	538	5,6
Sr^{1+}	550	5,7
Ca^{1+}	590	6,1
Y^{1+}	600	6,2
Bi^{1+}	703	7,3
Cu^{1+}	746	7,7
Ba^{2+}	965	10,0
Nd^{2+}	1040	10,8
Ce^{2+}	1050	10,9
Sr^{2+}	1064	11,0
La^{2+}	1067	11,1
Ca^{2+}	1145	11,9
Y^{2+}	1180	12,2
Bi^{2+}	1610	16,7
La^{3+}	1850	19,2
Ce^{3+}	1949	20,2
Cu^{2+}	1958	20,3
Y^{3+}	1980	20,5
Nd^{3+}	2130	22,1
Bi^{3+}	2466	25,6
Ce^{4+}	3547	36,8
Cu^{3+}	3555	36,8
Ba^{3+}	3600	37,3
Nd^{4+}	3900	40,4
Sr^{3+}	4138	42,9
Bi^{4+}	4370	45,3
La^{4+}	4819	49,9
Ca^{3+}	4912	50,9
Bi^{5+}	5400	56,0
Sr^{4+}	5500	57,0
Cu^{4+}	5536	57,4

Fig. 10. Ionization energies of the different atoms which are involved in the chemical arrangement for the doped chemical formulas summarized in Table 1.

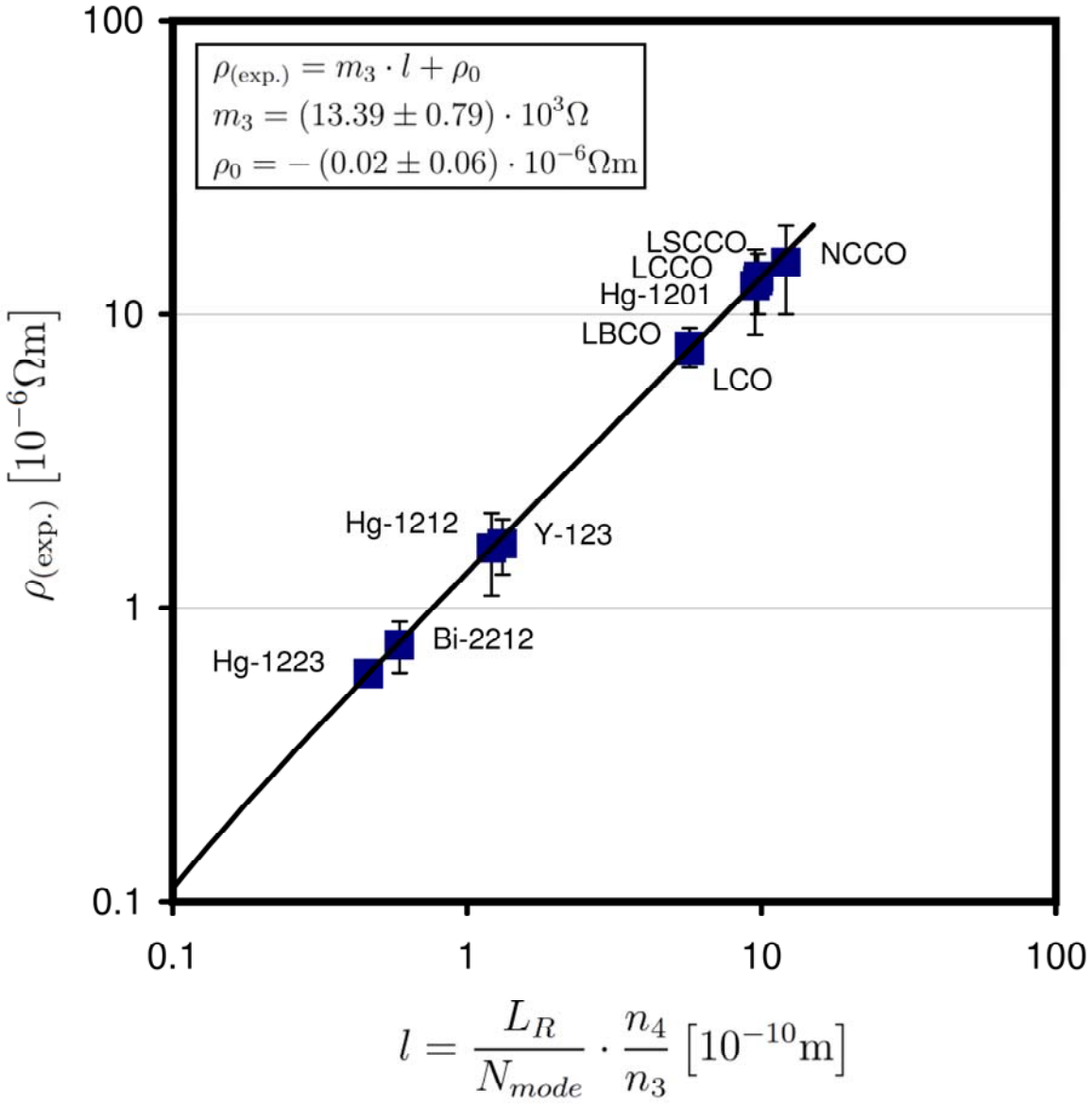

Fig. 11. The experimental resistivity at ~T_c has been plotted versus an effective length l for 10 different HTSCs. The transition temperature T_c varies between ~20 K (NCCO) and ~135 K (Hg-1223).

The superconducting unit volume has a size in the order of $V_{SC} \approx 10$ nm^3 and clearly shows size quantization. It is suggested that the superconducting unit volume is forming a waveguide for guiding superconducting carriers. The height of the waveguide is given by the distance between CuO_2 planes and the width is determined by the doping distance x as illustrated in Fig. 1 and 5-9 for several cases. Using the description of a waveguide for guiding superconducting carriers leads to the idea that the wave character of these carriers might be an adequate description for HTSC current channels. The concept has already been mentioned by considering a particle with mass, which is confined inside a box of width x, where its wave function satisfies the free-particle Schrödinger wave equation [1,40,41]. Maybe the transition between the normal state and the superconducting state at T_c marks the transition between the particle and the wave description.

Acknowledgements

We would like to thank J. Vernerey and H. Hall for discussions and valuable comments. This work is supported by the Friedrich-und-Elisabeth-BOYSEN-Stiftung.

REFERENCES

1. **H.P.Roeser, D.T.Haslam, J.S.López, M.F. von Schoenermark, M.Stepper, F.M.Huber, A.S.Nikoghosyan,** J. Supercond. and Novel Magn., **24**, 1443 (2011).
2. **H.Takagi, S.Uchida, Y.Tokura,** Phys. Rev. Lett., **62**, 1197 (1989).
3. **L.Gao, Y.Y.Xue, F.Chen, Q.Xiong, R.L.Meng, D.Ramirez, C.W.Chu,** Phys. Rev. B, **50**, 4260 (1994).
4. **R.Masini, R.Eggenhöffner, E.Bellingeri, E.Giannini, R.Vaccarone,** Appl. Phys. Lett., **68**, 2282 (1996).
5. **S.Datta,** Electronic transport in mesoscopic systems, Cambridge University Press, 1995, ISBN 0-521-41604-3
6. **T.Heinzel,** Mesoscopic Electronics in Solid State Nanostructures, Wiley-VCH, Weinheim, 2003, ISBN 3-527-40375-2
7. **Y.Sun, J.D.Guo, G.C.Xiong,** Physica C, **341-348**, 1857 (2000).
8. **Y.Sun, J.D.Guo, Y.Wang, G.C.Xiong,** Supercond. Sci. Technol., **14**, 607 (2001).
9. **Y.Morikawi, T.Sugano, A.Tsukamoto, C.Gasser, K.Nakanishi, S.Adachi, K.Tanabe,** Physics C, **303**, 65 (1998).
10. **T.Ito, Y.Nakamura, H.Takagi, S.Uchida,** Physica C, **185-189**, 1267 (1991).
11. **A.L.Solov'ev, V.M.Dmitriev,** Low Temp. Phys., **35**, 169 (2009).
12. **A.S.Alexandrov, V.N.Zavaritsky, S.Dzhumanov,** Phys. Rev. B, **69**, 052505 (2004).
13. **H.Claus, U.Gebhard, G.Linker, K.Röhberg, S.Riedling, J.Franz, T.Ishida, A.Erb, G.Müller-Vogt, H.Wühl,** Physica C., **200**, 271 (1992).
14. **H.Fujishiro, H.Teshima, M.Ikebe, K.Noto,** Physica C, **392-396**, 171 (2003).
15. **S.W.Tozer, J.L.Koston, E.M.McCarron,** Phys. Rev. B, **47**, 8089 (1993).
16. **W.K.Kwok, J.Fendrich, S.Fleshler, U.Welp, J.Downey, G.W.Crabtree,** Phys. Rev. Lett., **72**, 1092 (1994).
17. **J.H.Su, V.Chintamaneni, S.M.Mukhopadhyay, R.R.Revur, T.Pyles, S.Sengupta,** Supercond. Sci. Technol., **19**, L51 (2006).
18. **M.A.Crusellas, J.Fontcuberta, S.Pinol,** Phys. Rev. B, **46**, 1489 (1992).
19. **H.P.Roeser, F.M.Huber, M.F. von Schoenermark, F.Hetfleisch, M.Stepper, A.Moritz, A.S.Nikoghosyan,** Acta Astronaut., **65**, 289 (2009).
20. **M.Naito, S.Karimoto, A.Tsukada,** Supercond. Sci. Tech., **15**, 1663 (2002).
21. **L.Forro,** Phys. Lett. A, **179**, 140 (1993).
22. **T.T.M.Palstra, B.Batlogg, L.F.Schneemeyer, J.V.Waszczak,** Phys. Rev. Lett., 61, 1662 (1988).
23. **D.A.Huse, M.P.A.Fisher, D.S.Fisher,** Nature, **358**, 553 (1992).
24. **R.J.Cava, B.Batlogg, R.B. van Dover, J.J.Krajewski, J.V.Waszczak, R.M.Fleming, W.F.Peck, L.W.Rupp, P.Marsh, A.C.W.P.James, L.F.Schnemeyer,** Nature, **345**, 602 (1990).
25. **K.Kinoshita, H.Shibata, T.Yamada**, Physica C, **171**, 523 (1990).
26. **K.Kinoshita, F.Izumi, T.Yamada, H.Asano,** Phys. Rev. B, **45**, 5558 (1992).
27. **A.Fuertes, X.Obradors, J.M.Navarro, P.B.Gomez-Romero, N.Casan-Pastor, F.Perez, J.Fontcuberta, C.Miravitlles, J.Rodriguez-Carvajal, B.Martinez,** Physica C, **170**, 153 (1990).

28. **M.Hücker, Y.J.Kim, G.D.Gu, J.M.Tranquada, B.D.Gaulin, J.W.Lynn,** Phys. Rev. B, **71**, 094510 (2005).
29. C.**Ulrich, S.Kondo, M.Reehuis, H.He, C.Bernhard, C.Niedermeyer, F.Bouree, P.Bourges, M.Ohl, H.M.Ronnow, H.Takagi, B.Keimer,** Phys. Rev. B, **65**, 220507 (2002).
30. **H.P.Roeser, D.Haslam, F.M.Huber, S.Lopez, M.F. von Schoenermark, A.S.Nikoghosyan, J.Vernerey,** Acta Astronaut., **65**, 1179 (2009).
31. **K.Kinoshita, T.Yamada,** Phys. Rev. B, **46**, 9116 (1992).
32. **R.J.Cava, A.Santoro, J.J.Krajewski, R.M.Fleming, J.V.Waszczak, W.F.Peck, P.Marsh,** Physica C, **172**, 138 (1990).
33. **H.Shaked, J.D.Jorgensen, B.A.Hunter, R.L.Hitterman, K.Kinoshita, F.Izumi, T.Kamiyama,** Phys. Rev. B, **48**, 12941 (1993).
34. **H.P.Roeser, F.Hetfleisch, D.T.Haslam, J.S.López, M.Stepper, J.Vernerey, F.M.Huber, M.F. von Schoenermark, A.S.Nikoghosyan,** Acta Astronaut., **66**, 637 (2010).
35. **F.C.Chou, D.C.Johnston, S.W.Cheong, P.C.Canfield,** Physica C, **216**, 66 (1993).
36. **R.Suryanarayanan, O.Gorochov, M.S.R.Rao, L.Ouhammou, W.Paulus, G.Heger,** Physica C, **185-189**, 573 (1991).
37. **A.R.Moodenbaugh, Y.Xu, M.Suenaga,** Phys. Rev. B, **38**, 4596 (1988).
38. **J.G.Bednorz, K.A.Müller,** J. Phys. B, **64**, 189 (1986).
39. **J.G.Bednorz, K.A.Müller,** Rev. Mod. Phys., **60**, 585 (1988).
40. **J.W.Rohlf,** Modern Physics from α to Z^0, New York, John Wiley & Sons, Inc., 1994.
41. **H.P.Roeser, D.T.Haslam, J.S.López, M.F. von Schoenermark, M.Stepper, F.M.Huber, A.S.Nikoghosyan,** Acta Astronaut., **69**, 235 (2011).